FieldLight: Device-Free Indoor Human Localization Using Passive Visible Light Positioning and Artificial Potential Fields

Daniel Konings, *Member, IEEE*, Nathaniel Faulkner, Fakhrul Alam, *Senior Member, IEEE*, Edmund M.-K. Lai, *Senior Member, IEEE*, and Serge Demidenko, *Fellow, IEEE*

***Abstract*—Device-free or passive localization techniques allow positioning of targets, without requiring them to carry any form of transceiver or tag. In this paper, a novel device-free visible light positioning technique is proposed. It exploits the variation of the ambient light levels caused by a moving entity. The target is localized by employing a system of artificial potential fields associated with a set of photodiodes embedded into an indoor environment. The system does not require the existing lighting infrastructure to be modified. It also employs a novel calibration procedure that does not require labelled training data, thus significantly reducing the calibration cost. The developed prototype system is installed in three typical indoor environments consisting of a corridor, foyer, and laboratory and was able to attain median errors of 0.68m, 1.20m and 0.84m respectively. Through experimental results, the proposed VLP technique is benchmarked against an existing wireless RSSI-based device-free localization approach, and was able to attain a median error 0.63m lower than the wireless technique.**

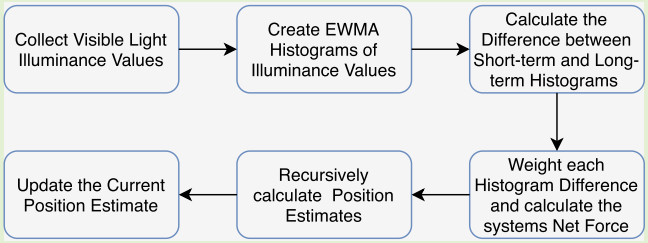

***Index Terms*—Indoor localization, visible Light positioning (VLP), device free localization (DFL), passive VLP, artificial potential fields.**

I. Introduction

ROBUST Location based services (LBS) for Smart Homes could enable personalized control of existing infrastructure including lighting, heating, air quality, and water temperature/flow [1], [2]. This could have a tremendous impact on wellbeing and assistive living as it would allow appliances to be controlled remotely. It could also be used to detect emergencies or falls, and automatically contact appropriate response personnel. This would thus enable the elderly to maintain higher autonomy, while providing the family the peace-of-mind of knowing that their elderly family members are safe and well.

While cameras can provide a suitable solution for public environments, they may create privacy concerns in residential areas. It is desirable also that the solution would utilize readily available hardware to facilitate ubiquitous deployment.

In the recent years, numerous wireless technology-based solutions have been proposed and reported in the literature. They utilized *Radio Tomographic Imaging* (RTI) [3]–[6], energy minimization [7], [8], and machine learning approaches (including: *Support Vector Machines* (SVM) [9], [10], Random Forest [11], *Hidden Markov Models* (HMM) [12], and Deep Learning [13]) to mention a few. These approaches are commonly implemented using either the *received signal strength indicator* (RSSI) metric, or the Wi-Fi *channel state information* (CSI) metric. CSI approaches have been shown to offer improved accuracy over RSSI approaches [14], however

Manuscript received August 22, 2019; accepted September 22, 2019. Date of publication September 27, 2019; date of current version December 31, 2019. This work was supported in part by Massey University Doctoral Scholarships. The associate editor coordinating the review of this article and approving it for publication was Prof. Bernhard Jakoby. *(Corresponding author: Daniel Konings.)*

D. Konings, N. Faulkner, and F. Alam are with the Department of Mechanical and Electrical Engineering, Massey University, Auckland 0632, New Zealand, and also with the School of Food and Advanced Technology, Massey University, Auckland 0632, New Zealand (e-mail: d.konings@massey.ac.nz; n.faulkner@massey.ac.nz; f.alam@massey.ac.nz).

E. M.-K. Lai is with the School of Engineering, Computer and Mathematical Sciences, Auckland University of Technology, Auckland 1142, New Zealand (e-mail: edmund.lai@aut.ac.nz).

S. Demidenko is with the School of Science and Technology, Sunway University, Selangor 47500, Malaysia, with the Department of MEE, Massey University, Auckland 0632, and also with the School of Food and Advanced Technology, Massey University, Auckland 0632, New Zealand (e-mail: s.demidenko@massey.ac.nz).

Digital Object Identifier 10.1109/JSEN.2019.2944178

the metric is not readily available in current Wi-Fi equipment and relies on legacy drivers [15], [16].

A major disadvantage of the wireless approaches is their potential vulnerability to malicious activities, which could lead to unlawful acquirement of location-based information from unsuspecting users, thus creating serious privacy concerns [17]. Other popular approaches include the use of passive infrared sensors [18], [19], load cells [20], capacitive sensing [21], electric field sensing [22]–[24], or microphone arrays [25]. The main concern with existing approaches is that they either require a significant deployment/calibration effort, or that they are not yet available as standard *commercial-off-the-shelf* (COTS) equipment. This makes it significantly more difficult to provide ubiquitous deployment of the wireless approaches for end users in the foreseeable future.

In recent years, *light-emitting diode* (LED) luminaires have become very popular light sources in indoor environments. In addition, they provide the opportunity to leverage the existing lighting infrastructure for a secondary purpose – indoor object localization (sensing). Visible light sensing applications can be classified into four groups: *full-active:* modified source and tagged target, *passive-src:* unmodified source and tagged target, *passive-obj:* modified source and untagged target, and *full-passive:* unmodified source and untagged target [26].

The focus of this paper is on implementing a full-passive localization system that does not require any modification of the lighting infrastructure to emit signals, and can localize tag-free targets. This offers unique challenges as full-passive systems either assume that a roaming entity fully absorbs the visible light as it occludes an area, or that the reflectance off the target follows a deterministic model. Since the reflectance is affected by the color worn by the target, calibration requirements should be kept minimal to allow for multi-entity calibration.

The CeilingSee approach reported in [27] employs a machine learning algorithm to infer an occupancy count. It can be technically categorized as full-passive since it utilizes commodity COTS luminaires having no communication functionalities, and can localize untagged targets. However, the proposed solution requires the existing luminaire driver boards to be modified to allow for the luminaires to act as light sensors.

Another solution is reported in [28] where the luminaire drivers are modified to output an ID number. Each luminaire is co-located with a *photodiode* (PD). During every cycle, the proposed system checks whether each PD's current values exceed a predefined threshold. This is used to detect whether a person is present at one of several predefined locations, or whether a door is open.

The LocaLight [29] prototype employs 3 ceiling mounted COTS luminaires, and 5 PDs located on the floor, to detect the shadow of a passing person. However, this solution only identifies the presence of people (static or walking in a straight line) rather than offering target level localization/tracking.

The novel *device-free localization* (DFL) *adaptive multi-target positioning* (AMTP) algorithm is proposed in [30]. It identifies locations of shadowed PDs on the floor, and then clusters them into groups. The clusters are used to identify probable targets. The main problem associated with this approach is the limited real-world experimental verification. Most of the provided results are based solely on simulation. However, the simulation is performed using somewhat unrealistic assumptions and models; making the approach questionable for a real-world smart home deployment.

The EyeLight solution [31] uses modulated ON-OFF keyed luminaires, co-located with PDs to detect targets crossing virtual light barriers, while the StarLight approach [32] employs custom designed lighting panels containing multiple LEDs with each LED being modulated separately. StarLight detects shadowed PDs by calculating the normalized frequency power change (for each PD-LED pair), considering them shadowed if they exceed a predefined threshold. A similar detection strategy is employed by LiSense in [33] that utilizes several ceiling-mounted modulated luminaires, and a multitude of floor-mounted PDs, to perform 3D skeleton reconstruction.

A simulation of visible light sensing is reported in [34], based on a multitude of luminaires collocated with PDs within an indoor environment. It proposes the use of either the likelihood-ratio test, or mean spectral radius, as the system variance indicators to enable indoor localization. The approach looks promising. However, no results of real-world experiments are provided in the paper. Besides, the number of luminaires assumed in the simulation is quite high (i.e., exceeding the quantity that would normally be deployed in a real-world premise).

In the Smart Wall solution [35], a target is localized by measuring the change it creates in the *received signal strength* (RSS) of the ambient light, at an array of PDs embedded in the wall. The system shows promising localization capability. However, it relies on extensive fingerprinting making it a less attractive option for real-world implementations.

Spring-relaxation is an energy minimization technique that aims to reach an equilibrium state within a system of springs [36]. It is realized by attaching a set of artificial springs to the roaming target, with the other spring ends being attached to known static locations. The system then iteratively works to find the global minima, where the net force applied by the springs to the target is minimized. Traditionally, the approach has been utilized to locate a sensor within a *wireless sensor network*(WSN) [37]. More recently, the concept was applied to the low-power and low-data-rate close proximity wireless *ad hoc* network-based DFL system described in [7]. It has also been applied to localize a PD-based tag for an active VLP system [38]. A Similar energy minimization technique (originally employed for robot path planning) is Artificial Potential Fields [39], [40]. Instead of using a spring notation, it models the localization problem as a set of attractive and repulsive forces, emitted from known locations.

Until now, the concept of potential fields have not been applied to visible light-based DFL. A particularly attractive benefit of DFL based on the potential fields approach is that potential fields are more computationally efficient than competing techniques such as particle filters [41], [42]. The approach also maintains the valuable benefit of a dynamically

TABLE I
FEATURE COMPARISON OF VISIBLE LIGHT POSITIONING SYSTEMS

Algorithm	Works without LED modulation	Does not require labelled training data	Localizes and tracks passive targets	Extra infrastructure Investment	Experimental verification
FieldLight	Yes	Yes	Yes	Low	2D localization + tracking
Smart Wall	Yes	No	Yes	Low	2D localization + tracking
CeilingSee	Yes	No	No	Low	Occupancy Count
Ibrahim et al	No	Unknown	No	Low	2D region detection
LocaLight	Yes	Yes	No	Low	1D position estimates
AMTP	No	Yes	localizes	Very High	Blocking LOS attenuates PD signal
EyeLight	No	Activity recognition requires labelled data	Yes	Medium	2D localization + tracking + activity recognition
StarLight	No	PD placement requires room layout	Yes	High	2D localization + 3D skeleton reconstruction
LiSense	No	Yes	Skeleton reconstruction	Very High	3D skeleton postures

assigned weighting scheme, which allows for high localization accuracy across varying target speeds.

A novel device-free localization approach employing *visible light* (VL-DFL) and artificial potential fields based localization is proposed in this paper, called FieldLight. The approach provides localization and tracking of targets without the need to modify the existing lighting infrastructure, and without the utilization of extensive labelled training data. It offers an overall superiority over the previous discussed techniques as demonstrated by the feature comparison given in Table I.

The main contributions of this papers work are summarized as follows:

1) A novel VL-DFL algorithm called FieldLight is developed which can localize and track targets using a set of potential fields attached to triggered photodiodes. To the extent of the authors' knowledge, this is the first reported work that applies the artificial potential fields approach to VL-DFL
2) A calibration procedure that does not require any labelled training data is proposed for the developed VL-DFL. This makes the system less labor intensive, and easy to deploy.
3) The performance of FieldLight is evaluated by implementing it in multiple full-scale environments. The impact of various parameters on the localization accuracy is investigated.
4) The localization accuracy of FieldLight is experimentally compared with an existing wireless DFL algorithm in the same environment. As far as the authors are aware, this is the first reported performance comparison between wireless- and visible light-based DFL techniques. FieldLight is demonstrated to be more accurate than a state of the art wireless DFL technique.

II. SYSTEM OVERVIEW

Assuming an environment where the ambient light level remains constant, the change in illuminance can be calculated as:

$$\Delta E = E_{T1} - E_{T0}, \tag{1}$$

where E_{T1} and E_{T0} represent two consecutive illuminance samples in time, measured in lux. Since the PDs are mounted on the walls rather than on the floor (as in the existing approaches, e.g., [29], [33]), the shadowing influence caused by a roaming target does not completely occlude the attenuated node, as the node receives dispersed multipath light components from a number of luminaires available within the environment. It is hypothesized that even though each node receives illumination from multiple sources, the impact from the closest sources remains dominant when the *field of view* (FOV) remains unobstructed. This suggests that if the shadowing target does not fully occlude the FOV, it would still have some proportional attenuation effect on the amount of light sensed by nearby PDs. To exploit this effect, FieldLight uses an energy minimization concept in the form of artificial potential fields, weighted by the attenuation seen at each receiving node. All symbols used in this manuscript to outline the FieldLight approach are included in Table II. Since FieldLight assumes that background ambient light level remains constant, care must be taken to either ensure the illumination is predominantly made up of artificial light sources with a constant output, or the system must be calibrated to account for the changes in sunlight over the course of the day. In this paper experiments were conducted during the early evening when sunlight was minimal. Another consideration is the reflectance properties of the roaming targets attire. FieldLight was trained using a subject wearing dark attire to minimize reflectance during the offline training phase.

Let $\mathcal{N}$ light sensing nodes be deployed around the perimeter of the monitored area, within an indoor environment (Fig. 1).

Each node contains a PD, wall mounted at 1.4 m above the ground, to ensure that no furniture occludes the line-of-sight path between the luminaires and nodes. The sensing nodes measure the illuminance of the visible light and employ their onboard wireless modules to relay the information to a centralized server. The server collects the illuminance values from all PDs, detects which ones have been shadowed, and uses this information to localize a roaming target.

The FieldLight system tracks a roaming target based on its relative position to known wall mounted PDs (shown as the red

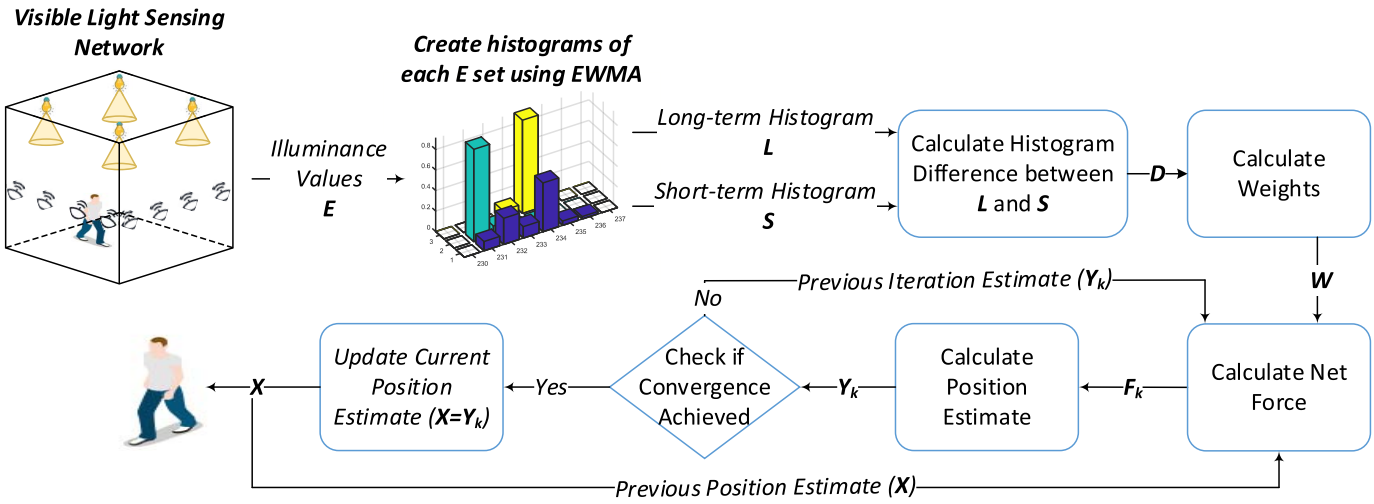

Fig. 1. FieldLight algorithm overview. **E** represents a stream of illuminance values for each wall mounted node. An exponentially weighted moving average (EWMA) scheme is used to create a long-term histogram (**L**) and a short-term histogram (**S**) for each node. The Bhattacharyya distance is taken between each nodes **L** and **S** histogram (**D**) which is used to generate a set of weights (**W**) for localization. The weights are used to calculate the net force on the system ($\mathbf{F}_k$), which continuously updates a position estimate ($\mathbf{Y}_k$) until the system either converges, or reaches its maximum iteration threshold. The final output position estimate for time t is then stored in **X**.

TABLE II
FIELDLIGHT SYMBOLS

Parameter	Description
E	Illuminance
β	Maximum attenuation constant
$\mathbb{D}$	Illuminance dataset
$\mathbb{h}$	Illuminance histogram
α	Smoothing factor
$\mathcal{I}$	Indication vector
$\mathbb{L}$	Illuminance histogram – long-term average
$\mathbb{S}$	Illuminance histogram – short-term average
$\mathcal{D}$	Histogram distance between $\mathbb{L}$ and $\mathbb{S}$
c	ln(0) constant
d	Euclidean distance
$\mathcal{X}$	Position estimate from previous timestep
n	Wall mounted node containing a photodiode
$\mathcal{W}$	Thresholding weight set
γ	Affected link threshold
$\mathcal{E}$	Geometric travel threshold
$\mathbb{W}$	Final weight set
$\mathcal{K}$	Maximum iteration constant
$\vec{\mathcal{F}}$	Net force
τ	Spring stepsize constant
$\mathcal{U}$	Spring energy threshold

circles in Fig. 2). The target does not carry any device (tag). Its presence is determined, and the target is located based on the visible light attenuation it causes to nearby nodes. A simplified side-view of the FieldLight setup is shown in Fig. 3.

The system implementing FieldLight operates in two stages. During the initial (offline) phase, the system collects two sets of readings. The first sample set consists of illuminance readings from all PDs when no target is present within the environment. The second sample set involves the target walking around the perimeter of the environment (as close as practically possible), ensuring that each PD is passed by. The system then calculates the maximum attenuation observed by each PD as a difference between the readings of the two sets. This results in the maximum reference threshold for each PD.

During the second (online) phase, the system uses the current illuminance sample to check which receiving nodes experience an attenuation that exceeds the established, predefined threshold. These nodes are then assigned as virtual field anchor points and they receive a weight based on the ratio between their current attenuation values, and the maximum attenuation calculated during the initial offline phase. The reasoning for this is that if a PD shows a similar level of attenuation to the offline maximum, it is likely that the target is within close proximity to the node. The iterative potential fields approach then uses each anchor with its associated weight, alongside the previous position estimate to converge on a new predicted location. This is done by assigning an attractive force to each of the affected nodes. An example of this is illustrated in Fig. 2(b), where the blue arrows represent the attractive forces.

III. ALGORITHM

As outlined in Section II, FieldLight requires the offline phase to determine the maximum attenuation threshold for each PD, followed by the online phase where a static or moving target is iteratively localized.

A. Offline Phase

To find the maximum attenuation value for each receiving node, the difference between the illuminance of the visible light in an ambient non-blocked and blocked (shadowed)

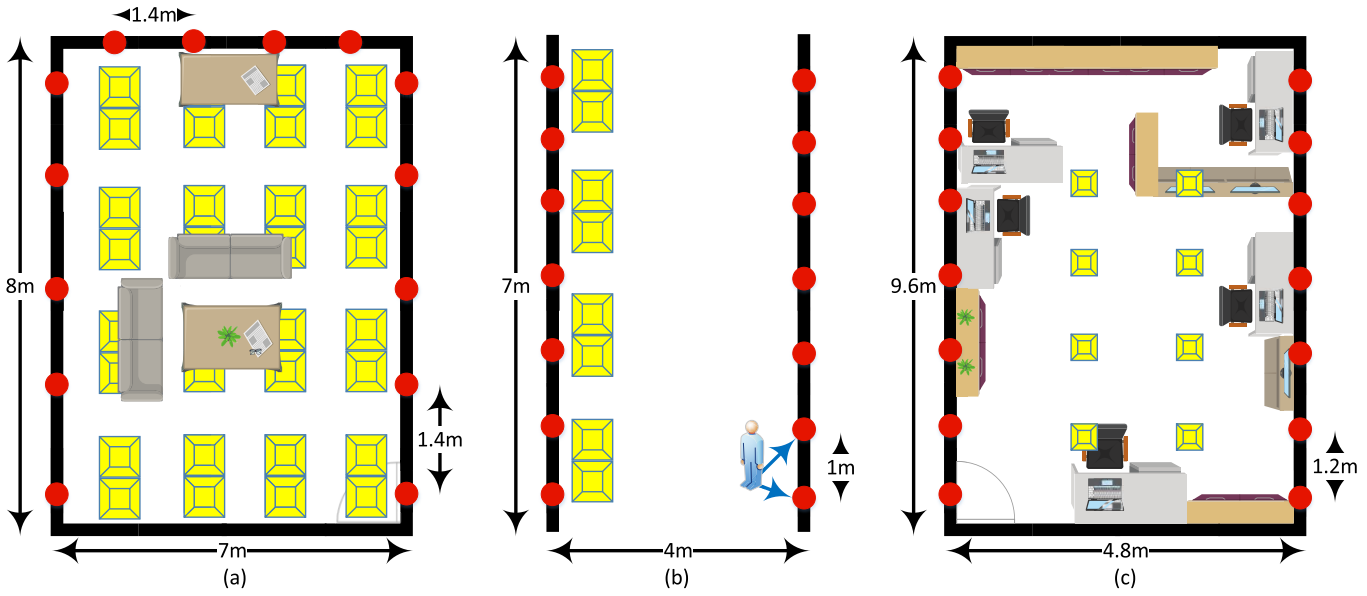

Fig. 2. FieldLight floorplan – (a) Foyer, (b) Corridor, (c) Laboratory. The yellow blocks represent the overhead luminaires used for localization. In each environment 14 nodes (red circles) were deployed which measured the changes in ambient light caused by a roaming entity and transmitted the information to a server for localization.

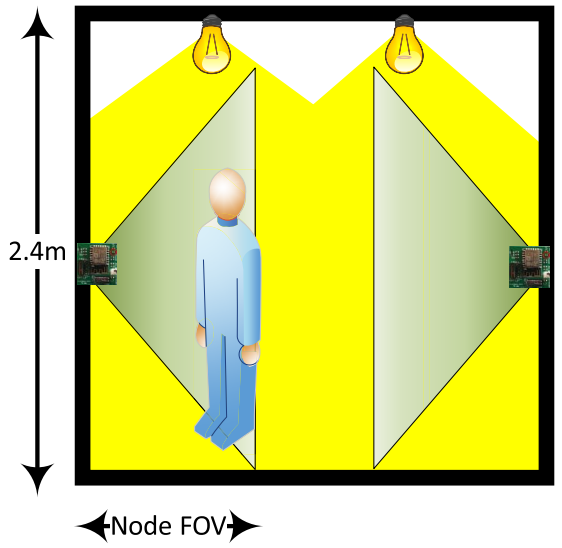

Fig. 3. Side-view of a person partially occluding the field of view of a wall mounted node.

conditions is calculated as:

$$\beta_n = \max_n \mathbb{D}_0 - \min_n \mathbb{D}_1, \tag{2}$$

where β_n is the scalar attenuation value at the nth receiving node, $\mathbb{D}_0$ is the offline illuminance dataset with no target within the environment, and $\mathbb{D}_1$ is the offline illuminance dataset containing a target roaming around the perimeter of the indoor site. The $\mathbb{D}_1$ dataset contains illuminance values recorded at the light sensors when a target is walking along the perimeter of the environment. Its minima value is associated with the target being within close proximity to a given node. This is achieved by taking the minimum value from the set. It is the largest attenuation experienced for the route, which is assumed to correlate with an entity passing nearby the node.

B. Online Phase

The FieldLight approach is based on the assumption that a roaming (or static) target prevents a portion of the ambient light from reaching nearby PDs placed on the walls in some fixed locations. To be able to calculate a target position from a set of raw E values (produced by PDs), an appropriate information feature (or metric) needs to be carefully chosen. It should be resilient to both varying environmental conditions, and random effects of a roaming entity. FieldLight utilizes histogram distances as it's metric. In the FieldLight approach, a set of long-term histograms ($\mathbb{L}$), that represent the background state of E at the PDs; and a set of short-term histograms ($\mathbb{S}$), which represent the current state are defined. The difference between the $\mathbb{L}$ and $\mathbb{S}$ histograms is the feature that is used as a representation of the target's presence. The number of bins used by each histogram is equivalent to the resolution of the PD-based sensing node. Assuming that the output signal of each PD is digitized into 1000 states, to represent E between 1-1000 lux, the corresponding value range is $[1, \mathbb{Z}]$, where $\mathbb{Z} = 1000$. Each histogram is therefore constructed with $\mathbb{Z}$ bins. The value contained in each histogram bin is based on the frequency of its respective illuminance value occurring within a stream of data. For example, a node recording an illuminance value of 319 lux will increase the value of the 319th bin, representing an increased occurrence rate of the 319 lux value. These values are then normalized to a frequency between 0-1 and weighted based on their time-of-arrival. An example of the histogram is shown in Fig. 4. When a person (or some other mobile object) passes near a PD, the $\mathbb{S}$ histogram quickly diverges from its steady-state values. Since the $\mathbb{L}$ histogram diverges slower (as shown in Fig. 4) the difference between the two can be used as a feature to detect an object's presence. To facilitate the use of the histogram distance feature, two histogram sets are created

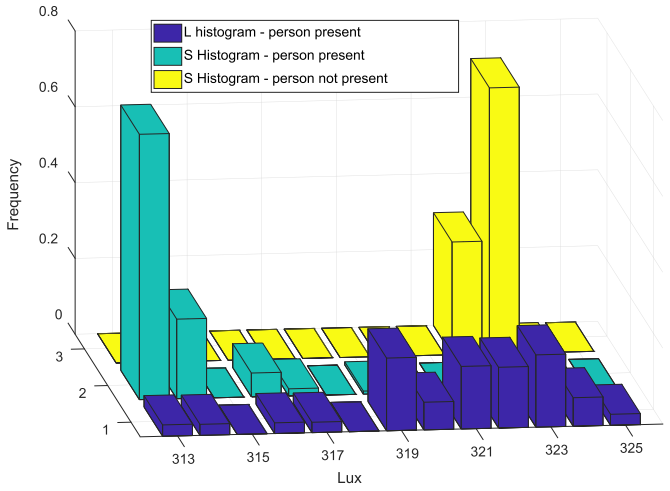

Fig. 4. The effect of a moving persons presence on both the Short-term ($\mathbb{S}$) and Long-term histograms ($\mathbb{L}$).

using an exponentially weighted moving average (EWMA) scheme using:

$$\mathbb{h}_n^t = (1-\alpha)\,\mathbb{h}_n^{t-1} + \alpha\hat{\mathfrak{J}}\left(E_n^t\right), \tag{3}$$

where: $\mathbb{h}_n^t$ is a histogram (with $\mathcal{Z}$ bins) for node n at the time t, with every value of the histogram being within ($\in [0,1]$); α is a constant smoothing factor ($\in [0,1]$); $\hat{\mathfrak{J}}$ is an indication vector of the length $\mathcal{Z}$ that returns 1 for the index given by illuminance value E_n^t, and 0 at every other position.

Bhattacharyya distance [43] is chosen as FieldLight's histogram distance metric as it can detect when the compared histograms have different standard deviations, even if their means are similar. This increases the sensitivity when a person (or object) is located near the edge of a PD's FOV thus causing very small changes to the node's received E values. In existing literature, Kernel and Kullback–Leibler distances have been used for histogram-based wireless localization [7], [44]. A recent study on various histogram distances showed that Bhattacharyya and Chi Squared distances perform well when used for a spring-relaxation based wireless approach [34]. Bhattacharyya distance provided the highest accuracy across all environments (e.g. 0.68m median error in the corridor environment vs 1.33m for Kernel distance and 2.69m for the Kullback-Leibler distance). It was therefore chosen as the distance metric.

By using (3) to formulate each histogram in $\mathbb{L}$ and $\mathbb{S}$ sets, while ensuring $\alpha_{\mathbb{S}} < \alpha_{\mathbb{S}}$, the Bhattacharyya distance between $\mathbb{L}$ and $\mathbb{S}$ can be defined as:

$$\mathcal{D}_n = -\ln\left(c + \sum\sqrt{\mathbb{L}_n \cdot \mathbb{S}_n}\right), \tag{4}$$

where: $\mathbb{L}_n$ and $\mathbb{S}_n$ represent the long-term and short-term histograms for node n, created using (3), respectively; $\cdot$ is the *dot product*, the small constant term c is added to ensure that no $\ln(0)$ error occurs if no bin values overlap between the $\mathbb{L}$ and $\mathbb{S}$ histograms.

After a distance metric has been defined, thus enabling FieldLight to detect changes occurring around the nodes due to object movement, a selection criterion is established to identify and pick only the strongly impacted nodes, and to weigh them accordingly. This is achieved by using a thresholding process, utilizing: the Bhattacharyya distance for each node ($\mathcal{D}_{1:\mathcal{N}}$), and $d(\mathcal{X}, n)$, where $d(\mathcal{X}, n)$ is defined as the *Euclidean distance* between the previous position estimate $\mathcal{X}$, and the node n. When FieldLight is first turned on, $\mathcal{X}$ is initialized to the coordinate of the center of the entry doorway. Through the thresholding, FieldLight collects two weights for each receiving node.

The first weight is defined by:

$$\mathcal{W}_n^1 = \begin{cases} \mathcal{D}_n, & \mathcal{D}_n > \gamma \\ & \text{and } d(\mathcal{X}, n) < \mathcal{E} \\ 0, & \text{otherwise,} \end{cases} \tag{5}$$

where: γ and $\mathcal{E}$ are predefined thresholding constants, with γ ensuring that only strongly affected links are selected, while $\mathcal{E}$ provides a geometric restriction on the maximum level of target movement allowed between the chosen time steps.

The second weight uses the same thresholding condition. However, it stores the current attenuation as a proportion of the offline calibration value β_n:

$$\mathcal{W}_n^2 = \begin{cases} \dfrac{|mode(\mathbb{L}_n) - mode(\mathbb{S}_n)|}{\beta_n}, & \mathcal{D}_n > \gamma \\ & \text{and } d(\mathcal{X}, n) < \mathcal{E} \\ 0, & \text{otherwise,} \end{cases} \tag{6}$$

where the $mode()$ function returns the modal value (i.e. the bin index with the largest value) of a given histogram.

After the weights are calculated for all receiving nodes, the two weight sets are combined into a single set as:

$$\mathbb{W} = \frac{(\mathcal{W}^1 \circ \mathcal{W}^2) - \min(\mathcal{W}^1 \circ \mathcal{W}^2)}{\max(\mathcal{W}^1 \circ \mathcal{W}^2) - \min(\mathcal{W}^1 \circ \mathcal{W}^2)}, \tag{7}$$

where $\circ$ is the *Hadamard product*. This is performed to normalize the weight sets since $\mathcal{W}^1$ and $\mathcal{W}^2$ have different ranges, and maximum values.

After the histogram distances and weights are calculated for each receiving node, FieldLight implements an iterative potential fields procedure to both localize and track a moving target. The maximum number of iterations per the time step is defined in advance by the constant $\mathcal{K}$.

In a single iteration, the FieldLight computes an attractive force between the previous target position estimate, and each affected node. The net force within the system is calculated by summing the forces across the overlapping potential fields using:

$$\vec{\mathcal{F}}_k = \tau \sum_{n=1}^{\mathcal{N}} \vec{\mathcal{X}}_n \mathbb{W}_n, \tag{8}$$

where: k represents a single iteration (k iterates from $0:\mathcal{K}$); $\vec{\mathcal{X}}_n$ is a vector between the previous position estimate $\mathcal{Y}_{k-1}$ and the position of the nth receiving node; τ is a scaling constant.

In each iteration, the current position estimate is given using:

$$\mathcal{Y}_k = \begin{cases} \mathcal{X}, & k = 0 \\ \mathcal{Y}_{k-1} + \vec{\mathcal{F}}_k, & k > 0, \end{cases} \tag{9}$$

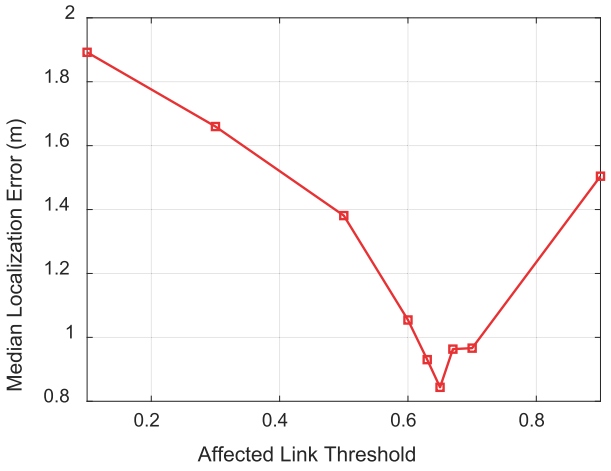

Fig. 5. Impact of affected link threshold, γ, on FieldLight's performance (shown as median localization error). Laboratory environment.

where $\mathcal{X}$ is the position estimate from the previous time step. The final position estimate for the current time step can then be found as:

$$\mathcal{X} = \begin{cases} \mathcal{Y}_k, & \left|\vec{\mathcal{F}}_k\right| < \mathcal{U} \text{ and } k < \mathcal{K} \\ \mathcal{Y}_{\mathcal{K}}, & k = \mathcal{K}, \end{cases} \tag{10}$$

where $\mathcal{U}$ is the efficiency threshold that is used to terminate the potential fields algorithm early if the field equilibrium has already been reached (i.e., the net force on the system is small enough).

IV. Parameter Tuning

For FieldLight to perform adequately, its parameter values need to be carefully tuned to optimize the localization accuracy. In this manuscript all localization errors are calculated by taking the Euclidean distance between the ground truth and estimated positions. Fig. 5 and Fig. 6 show how varying parameter values affect the overall localization accuracy within the laboratory environment (Fig. 2(c)1/Fig. 7). The results for the laboratory environment comparison is given here since the LED luminaires were utilized in it for illumination – the same as in most *visible light positioning* (VLP) approaches presented in the literature.

The parameters shown in Fig. 5 and Fig. 6 were initialized to the values used for wireless histogram localization in [7], [44], [45]. Each parameter was then manually tuned while keeping all others at their initial value. A recorded illuminance dataset from each environment was used to ascertain which of the parameter changes produced the largest positive influence on the overall localization error. The parameter with the largest positive change was then re-initialized to the new tuned value. The manual tuning was then repeated for all other parameters, fixing one parameter to its new optimum value each round. This was repeated until all parameters had been tuned.

After empirically tuning the parameter values for each environment, it was discovered that most parameters were environmentally agnostic. This means that though the Affected link threshold (γ) was needed to be tuned for each environment, the other parameter values could be kept constant, which would minimize the required user input during the calibration process. As it could be seen in Fig. 6, there is a wide "optimum" range within which the parameters provide adequate performance. For example, $\alpha_{\mathcal{L}}$ has an acceptable range between 0.03-0.05, $\alpha_{\mathcal{S}}$ - between 0.6-0.75, τ - between 0.05-0.09, and $\mathcal{U} < 0.06$.

TABLE III
FieldLight Parameters

Parameter	Description	Value
$\alpha_{\mathcal{L}}$	Smoothing Factor – Long-term	0.03
$\alpha_{\mathcal{S}}$	Smoothing Factor – Short-term	0.7
c	ln(0) Factor	0.00001
γ_{Foyer}	Affected Link Threshold	0.7
$\gamma_{Corridor}$	Affected Link Threshold	1.05
$\gamma_{Laboratory}$	Affected Link Threshold	0.65
$\mathcal{E}$	Geometric Travel Threshold	5
$\mathcal{K}$	Maximum Iteration Constant	6
τ	Stepsize Constant	0.06
$\mathcal{U}$	Energy Threshold	0.05

Fig. 8 shows an example of the distance that the target position estimate is updated by, with each iteration. For example, if FieldLight has updated its position estimate 4 times within the current timestep (*iteration index* = 4), the *distance moved* represents $\mathcal{Y}_4 - \mathcal{Y}_3$. As shown in Fig. 8, the distance moved decreases with each iteration, as FieldLight converges towards its final position estimate for the current timestep. The experiment was based on the extreme case where the previous position estimate was far away from the current location. The algorithm did not finish converging after 50 iterations. At the same time, by using 6 as a value of $\mathcal{K}$ (Table III) and 0.07m as an average iteration step, while also employing the 10Hz E sample rate, the system can accommodate a maximum target roaming speed of 4.2m/s. Since this is already significantly higher than the average adult walking speed (1.4m/s), the full convergence is not actually required. Besides, achieving the full convergence would introduce an unnecessary computational burden. This shows that careful considerations should be undertaken when deploying the FieldLight system, as the required maximum iteration number is intrinsically linked to both the desired performance level, and the overall network speed.

V. Experimental Setup and Results

The FieldLight hardware consists of 14 wall mounted custom boards that were designed to take ongoing readings of the perceived light level at a 10Hz sampling rate, and then wirelessly transmit these reading to the dedicated processing server, consisting of a laptop with an intel i7 processor, running windows 10 [35]. Preliminary tests performed with the nodes mounted within a range of heights of 0.75m-1.4m show no noticeable impact on the localization accuracy. The sensors

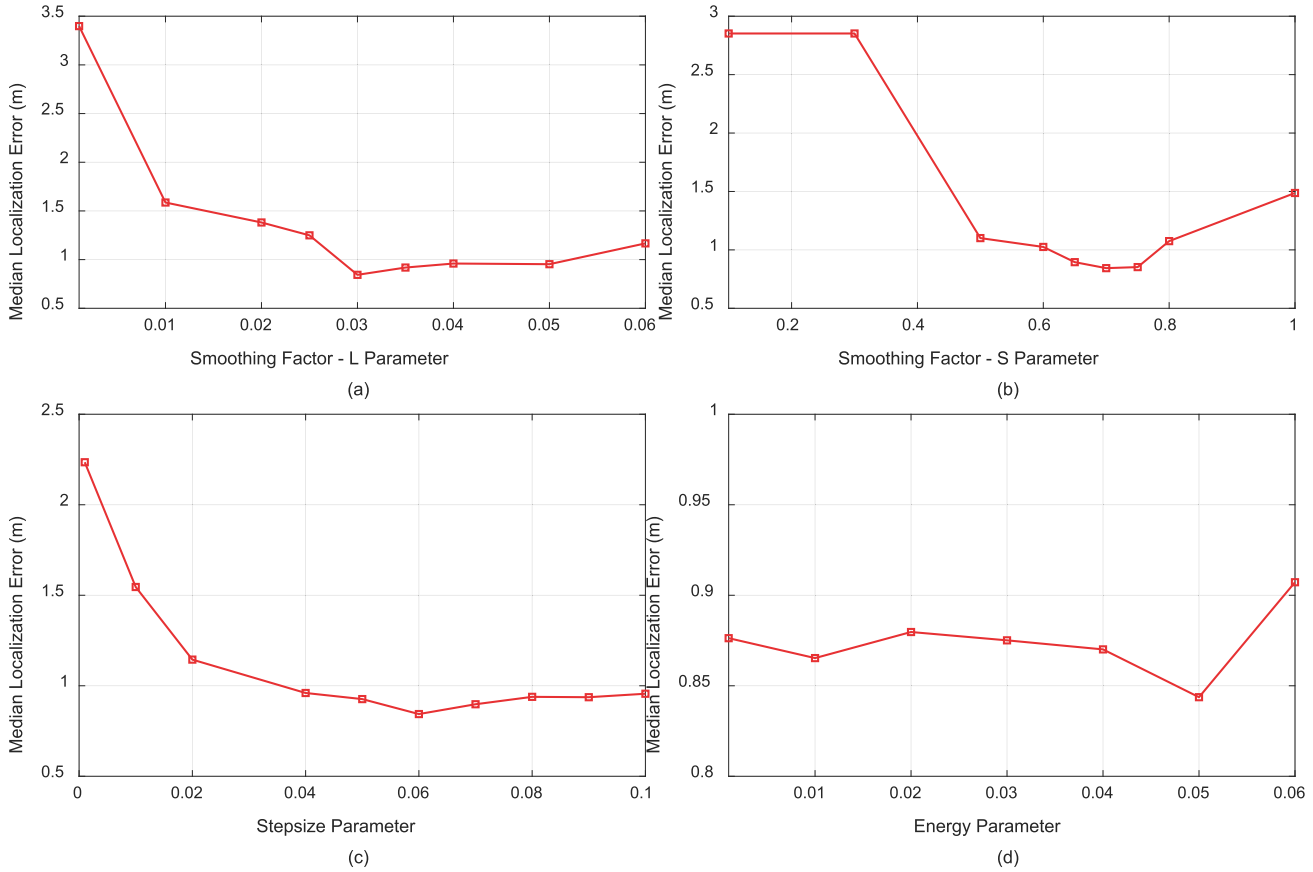

Fig. 6. The effect of varying parameter values on FieldLight's performance (shown as median localization error) for the Laboratory environment.

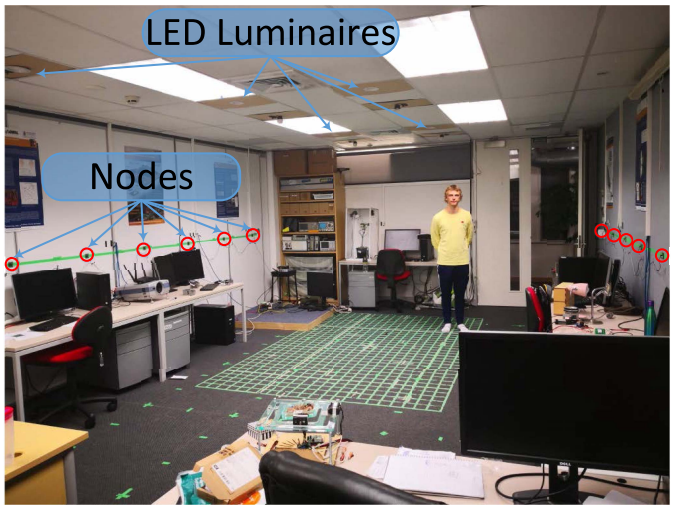

Fig. 7. FieldLight Laboratory environment. The fluorescent tubes shown were only turned on to produce a clear image. During experiments, only the LED luminaires were turned on.

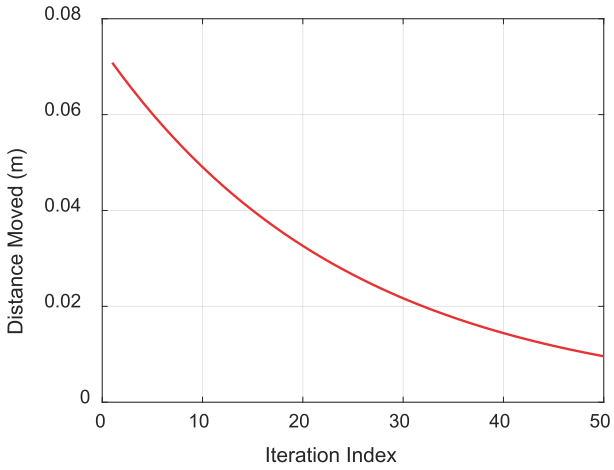

Fig. 8. An example of FieldLights iterative convergence approach, for a target that has travelled a significant distance since the previous timestep. The 'Distance Moved' represents how much the output position estimate is updated for each iteration of FieldLight.

were eventually mounted at 1.4m high to ensure that they were above the room furniture, to avoid occlusions.

Since the nodes are detecting changes in ambient light, they do not need to be placed relative to the light bulbs. However, careful placement is required to ensure coverage. In our experiments, we discovered that the sensors register a measured change in RSS level for approximately 3m-4m distance from the wall itself. This means that larger rooms will require either ceiling mounted, or floor mounted sensors (or fusion with another technology like wireless) to extend the coverage to the center of the room.

The custom boards (receiving nodes) consist of the Renesas Electronics ISL29023 Digital Ambient Light Sensor connected

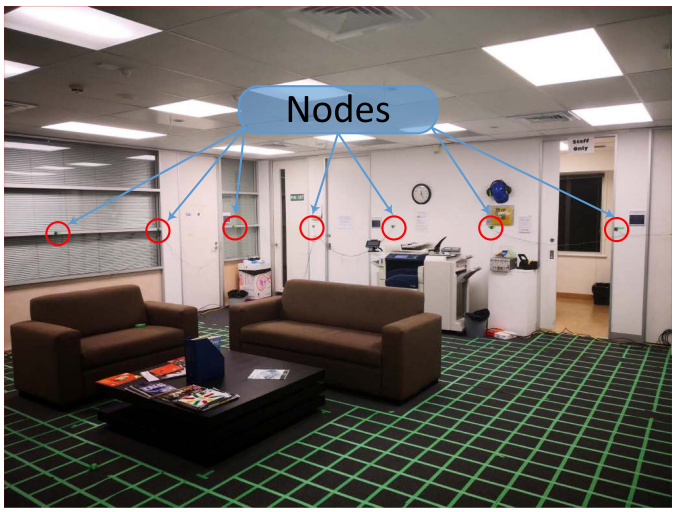

Fig. 9. FieldLight Foyer environment.

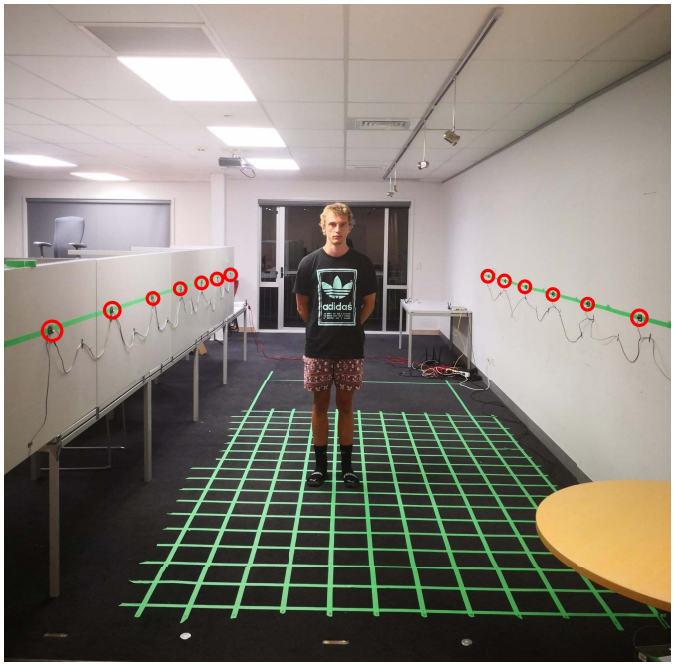

Fig. 10. FieldLight Corridor environmentm.

to an ESP 8266 microcontroller sampling the PD output, and sending the data to the processing server over Wi-Fi. The ISL29023 offers the onboard 50/60Hz flicker rejection and UV rejection. It is also very affordable, thus facilitating the potential for ubiquitous system adoption within smart home environments (the prototype cost remains below USD 5 per sensor node). It is envisioned that the sensors will be embedded within the walls, operating on mains power with the power cables running behind the wall panels like regular power conduits. Since only the photodiode will be visible on the wall, this will not be conspicuous, and will not have an unfavorable effect on an environments aesthetics. Once VLC adoption becomes widespread, many smart appliances will be equipped with VLC receivers (e.g. smart TV/fridge). Since these appliances are commonly positioned against walls and run off the mains power, they could potentially be used to provide a secondary localization benefit, without requiring the sensors to be embedded within the walls at those locations.

The custom boards, were mounted on the walls in 3 experimental environments (Fig. 2): a 7m $\times$ 8m foyer (Fig. 9) with 1.4m node spacing, a 4m $\times$ 7m corridor (Fig. 10) with 1m node spacing, and a 4.8m $\times$ 9.6m laboratory (Fig. 7) with 1.2m node spacing. All experiments were undertaken in the evening so that the overhead luminaires provided all the illumination within each test environment. The corridor and foyer employed fluorescent tubes for illumination while the laboratory utilized REX10CDLDIM LED luminaires. The LED luminaires had a rated power of 13W, beam angle of 90°, and were driven by a constant current of 350mA. The fluorescent lights seen in Fig. 7 were not turned on during the experiments at the laboratory.

To calibrate the system during the offline phase, a 1.84m tall subject moved around the perimeter of each site (as close as possible to the walls, while navigating around the furniture). The E values were collected from each receiving node at a 10Hz rate. The parameters of FieldLight were optimized using empirical tuning, and the employed final values are given in Table III.

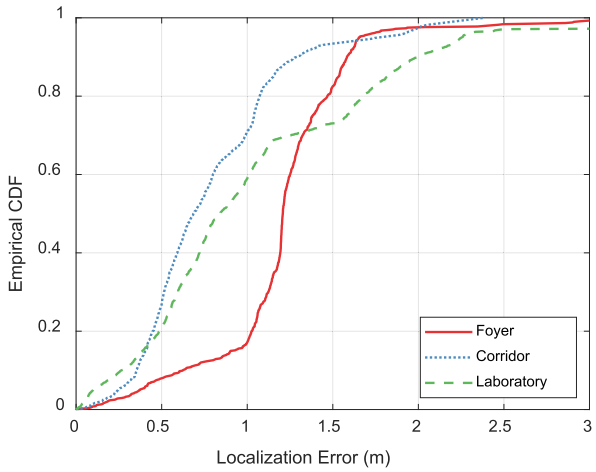

Fig. 11. FieldLight localization performance in all experimental environments.

During the online phase, the target walked along a marked path through each of the environments in a heel-toe fashion at 0.78m/s, with the steps being synchronized to a metronome. Illuminance values were recorded of the subject walking 3 times in each direction along the marked path, which was combined to form a single dataset. This ensured that both the step size and walking speed remained constant, and the ground truth location was known at each time step. One of the trials showing the ground truth path and estimated paths for each environment is shown in Fig. 12, Fig. 13 and Fig. 14. In the corridor, foyer, and laboratory environments, FieldLight achieved median errors of 0.68m, 1.20m, and 0.84m respectively. The *cumulative distribution function* (CDF) of the localization error for all the three test locations are shown in Fig. 11, and the median/95$^{\text{th}}$ percentile errors are shown

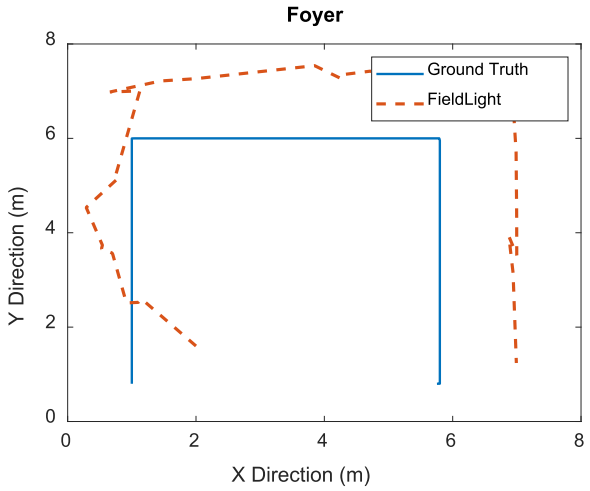

Fig. 12. Ground truth path and FieldLight position estimates from a single trial in the Foyer environment.

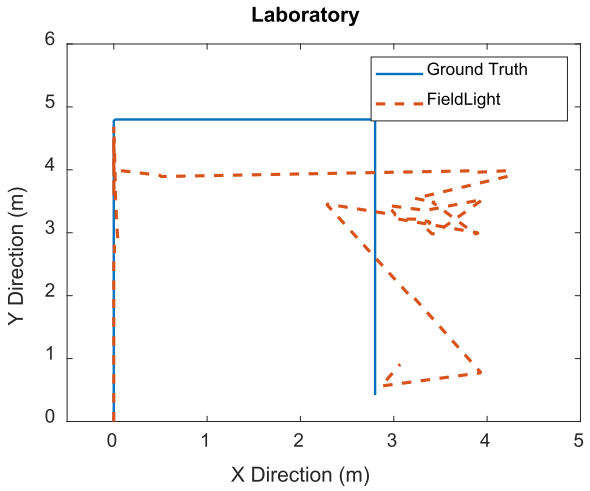

Fig. 14. Ground truth path and FieldLight position estimates from a single trial in the Laboratory environment.

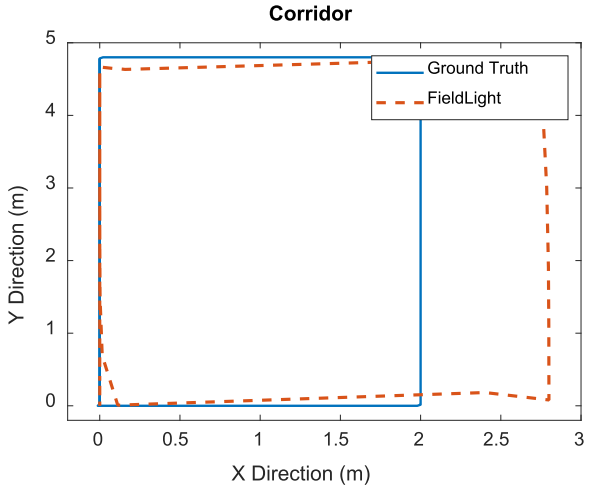

Fig. 13. Ground Truth path and FieldLight position estimates from a single trial in the corridor.

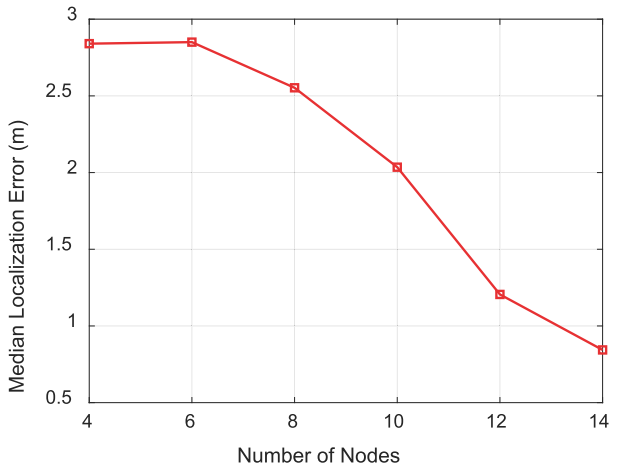

Fig. 15. Impact of number of light sensors on FieldLight's performance (shown as median localization error) in laboratory environment.

TABLE IV
FIELDLIGHT LOCALIZATION PERFORMANCE

Environment	Standard Deviation (m)	Minimum Error (m)	Median Error (m)	95th Percentile Error (m)	Maximum Error (m)
Foyer	1.40	0.04	1.20	1.65	8.83
Corridor	0.43	0.02	0.68	1.77	2.38
Laboratory	0.91	0.01	0.84	2.25	5.41

in Table IV. Interestingly, the performance in the clear corridor was similar (within 0.2m error difference) to the cluttered laboratory for the first two error quartiles (Fig. 11). This suggests that a cluttered environment has stronger negative influence in areas where localization performance is already poor. Another key observation was that the localization ability in the foyer was significantly inferior to that in the other two environments. This was mainly caused by the larger dimension of the foyer. In both the corridor and laboratory environments, the walking subject always remains within 3m of a PD. However, in the foyer, the target walking through the middle of the room was over 3.5m away from the nearest PD. The impact of the traversing person on the RSS was extremely low at this distance creating dead spots where the node is not capable to pick up the motion. This resulted in the erroneous output estimates.

The effect of reducing the number of receiving nodes employed for the localization is shown in Fig. 15. As expected, the localization accuracy decreases with fewer nodes.

To demonstrate how the FieldLight compares to the existing wireless-based approaches, that can be implemented using modern COTS equipment, it was benchmarked against SpringLoc [7]. SpringLoc has been proven to be one of the most accurate approaches among the DFL techniques that use the wireless RSSI metric. The laboratory environment (Fig. 7) was chosen for the comparison. SpringLoc uses a spring relaxation based DFL approach. It employs the Zigbee *received signal strength indicator* (RSSI) metric and creates virtual anchors within the environment, rather than employing the nodes themselves as anchors. The same number of nodes (14 nodes, each placed on the walls at a height of 1.4 m)

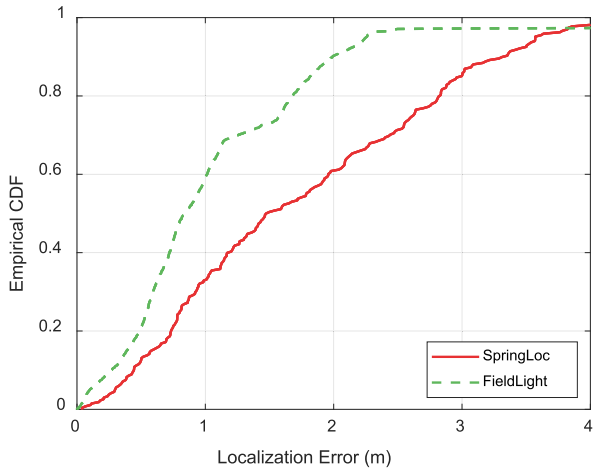

Fig. 16. FieldLight vs SpringLoc in the laboratory environment.

TABLE V
FIELDLIGHT VS SPRINGLOC PERFORMANCE

Algorithm	Standard Deviation (m)	Minimum Error (m)	Median Error (m)	95th Percentile Error (m)	Maximum Error (m)
FieldLight	0.91	0.01	0.84	2.25	5.41
SpringLoc	1.09	0.04	1.47	3.57	4.86

were utilized for both the approaches. FieldLight used the PD-based sensors whereas SpringLoc utilized Texas Instrument CC2530 Zigbee radios.

The visible light based FieldLight surpassed the localization accuracy of the wireless SpringLoc approach as shown in Fig. 16 and Table V, when compared to the ground truth path. However, at the 98th-100th bands, SpringLoc approach displayed higher accuracy. This was because the wireless signals can operate in non-line of sight scenario, whereas the visible light-based nodes rely on the line of sight light paths. This means that in some cases FieldLight could suffer from a few large localization errors. For example, consider the entrance to the work area shown in the top right corner of Fig. 2(c). The ambient light level in this region is lower as there are significant furniture items obstructing the light propagation. When traversing this region, a roaming entity had a negligible impact on the nearby PDs, which contributed to several large localization errors in small areas, creating dead spots. The impact of this is shown in the top right corner of Fig. 14, as the target was temporarily lost as it passed in front of the occluding office furniture.

VI. CONCLUSION AND FUTURE WORKS

Existing VLP approaches require either a tagged subject, extensive infrastructure modifications, or significant offline training effort. FieldLight removes these limitations, while still providing at least a 1.2m median localization accuracy

within multiple indoor environments. The research confirms that practical device-free VLP systems are plausible. However, further work is to be done to expand FieldLight to enable multiple targets tracking. FieldLights potential fields approach is not computationally complex, and the current factor limiting the maximum target speed is the 10Hz sample rate. If the system is required to track faster targets, either the sampling rate can be increased, at the cost of energy efficiency, or the stepsize constant can be increased, at the cost of low speed accuracy. Furthermore, FieldLight assumes there is a linear relationship between the portion of a nodes FOV that is affected by a target, and the total level of attenuation perceived. If more precise models are developed to accurately model this relationship, the overall localization accuracy could be improved. FieldLight was calibrated while the target wore a black t-shirt. While the system remains functional for multiple apparel colors, the performance would degrade. This could be addressed by utilizing multiple training models, for multiple colored apparels. Finally, FieldLight's performance degrades because of the dead spots caused by the subject traversing outside the sensing region of nearby nodes. Earlier work has reported that roof mounted nodes can measure the change in ground reflection to detect targets [27]. This suggests that careful node placement along both the roof and walls can potentially be used to ensure adequate coverage and optimize overall localization accuracy. Another option could involve fusing the FieldLight with a wireless DFL system to help remove the dead spots, as supported by the 98th-100th bands of SpringLoc, though more comparative tests are required to quantify the benefit a fused system could bring. Furthermore, the RSSI metric used by SpringLoc is a coarse metric when compared to Wi-Fi CSI. If CSI ever became readily accessible in COTS equipment, a fused system with CSI and visible light may bring further benefits. Finally, FieldLight uses potential fields as it is a computationally efficient method of providing localization, when compared to competing particle filters. However, potential fields approaches could potentially converge at incorrect local minimum, if the deployment area was large. It would be interesting to try detect these cases, and employ a backup algorithm (such as a particle filter) to ensure correct convergence.

REFERENCES

[1] A. Schieweck, E. Uhde, T. Salthammer, L. C. Salthammer, L. Morawska, M. Mazaheri, and P. Kumar, "Smart homes and the control of indoor air quality," *Renew. Sustain. Energy Rev.*, vol. 94, pp. 705–718, Oct. 2018.

[2] H. Huang, G. Gartner, J. M. Krisp, M. Raubal, and N. Van de Weghe, "Location based services: Ongoing evolution and research agenda," *J. Location Based Services*, vol. 12, no. 2, pp. 63–93, 2018. doi: 10.1080/17489725.2018.1508763.

[3] H. Yiğitler, R. Jäntti, O. Kaltiokallio, and N. Patwari, "Detector based radio tomographic imaging," *IEEE Trans. Mobile Comput.*, vol. 17, no. 1, pp. 58–71, Jan. 2016.

[4] O. Kaltiokallio, R. Jantti, and N. Patwari, "ARTI: An adaptive radio tomographic imaging system," *IEEE Trans. Veh. Technol.*, vol. 66, no. 8, pp. 7302–7316, Aug. 2017.

[5] Q. Wang, H. Yiğitler, R. Jäntti, and X. Huang, "Localizing multiple objects using radio tomographic imaging technology," *IEEE Trans. Veh. Technol.*, vol. 65, no. 5, pp. 3641–3656, May 2016.

[6] X. Shengxin, L. Heng, G. Fei, and W. Zhenghuan, "Compressive sensing based radio tomographic imaging with spatial diversity," *Sensors*, vol. 19, no. 3, p. 439, 2019.

[7] D. Konings, F. Alam, F. Noble, and E. M.-K. Lai, "SpringLoc: A device-free localization technique for indoor positioning and tracking using adaptive RSSI spring relaxation," *IEEE Access*, vol. 7, pp. 56960–56973, 2019.

[8] J. Wang *et al.*, "Transferring compressive-sensing-based device-free localization across target diversity," *IEEE Trans. Ind. Electron.*, vol. 62, no. 4, pp. 2397–2409, Apr. 2015.

[9] R. Zhou, X. Lu, P. Zhao, and J. Chen, "Device-free presence detection and localization with SVM and CSI fingerprinting," *IEEE Sensors J.*, vol. 17, no. 23, pp. 7990–7999, Dec. 2017.

[10] X. Dang, Y. Huang, Z. Hao, and X. Si, "PCA-Kalman: Device-free indoor human behavior detection with commodity Wi-Fi," *EURASIP J. Wireless Commun. Netw.*, vol. 2018, no. 1, p. 214, 2018.

[11] H. Zou, Y. Zhou, J. Yang, W. Gu, L. Xie, and C. Spanos, "FreeDetector: Device-free occupancy detection with commodity WiFi," in *Proc. IEEE Int. Conf. Sens., Commun. Netw. (SECON Workshops)* Jun. 2017, pp. 1–5. doi: 10.1109/SECONW.2017.8011040.

[12] H. Zhang *et al.*, "Wireless non-invasive motion tracking of functional behavior," *Pervasive Mobile Comput.*, vol. 54, pp. 29–44, Mar. 2019.

[13] X. Wang, L. Gao, S. Mao, and S. Pandey, "CSI-based fingerprinting for indoor localization: A deep learning approach," *IEEE Trans. Veh. Technol.*, vol. 66, no. 1, pp. 763–776, Jan. 2017. doi: 10.1109/tvt.2016.2545523.

[14] Z. Yang, Z. Zhou, and Y. Liu, "From RSSI to CSI," *ACM Comput. Surv.*, vol. 46, no. 2, pp. 1–32, 2013.

[15] Y. Xie, Z. Li, and M. Li, "Precise power delay profiling with commodity Wi-Fi," in *Proc. 21st Annu. Int. Conf. Mobile Comput. Netw. MobiCom*, Paris, France, 2015, pp. 53–64. doi: 10.1145/2789168.2790124.

[16] D. Halperin, W. Hu, A. Sheth, and D. Wetherall, "Tool release," *ACM SIGCOMM Comput. Commun. Rev.*, vol. 41, no. 1, p. 53, 2011.

[17] G. Sun, Y. Xie, D. Liao, H. Yu, and V. Chang, "User-defined privacy location-sharing system in mobile online social networks," *J. Netw. Comput. Appl.*, vol. 86, pp. 34–45, May 2007.

[18] D. Yang, W. Sheng, and R. Zeng, "Indoor human localization using PIR sensors and accessibility map," in *Proc. IEEE Int. Conf. Cyber Technol. Automat., Control, Intell. Syst. (CYBER)*, Jun. 2015, pp. 577–581.

[19] J. Kemper and H. Linde, "Challenges of passive infrared indoor localization," in *Proc. 5th Workshop Positioning, Navigat. Commun.*, Mar. 2008, pp. 63–70.

[20] G. Mokhtari, N. Bashi, Q. Zhang, and G. Nourbakhsh, "Non-wearable human identification sensors for smart home environment: A review," *Sensor Rev.*, vol. 38, no. 3, pp. 391–404, Jun. 2018. doi: 10.1108/SR-07-2017-0140.

[21] O. B. Tariq, M. T. Lazarescu, J. Iqbal, and L. Lavagno, "Performance of machine learning classifiers for indoor person localization with capacitive sensors," *IEEE Access*, vol. 5, pp. 12913–12926, 2017.

[22] X. Tang and S. Mandal, "Indoor occupancy awareness and localization using passive electric field sensing," *IEEE Trans. Instrum. Meas.*, to be published.

[23] B. Fu, F. Kirchbuchner, J. von Wilmsdorff, T. Grosse-Puppendahl, A. Braun, and A. Kuijper, "Performing indoor localization with electric potential sensing," *J. Ambient Intell. Humanized Comput.*, vol. 10, no. 2, pp. 731–746, Feb. 2019.

[24] T. Grosse-Puppendahl *et al.*, "Platypus: Indoor localization and identification through sensing of electric potential changes in human bodies," in *Proc. 14th Annu. Int. Conf. Mobile Syst., Appl., Services*, Jun. 2016, pp. 17–30.

[25] T. Kivimäki, T. Vuorela, P. Peltola, and J. Vanhala, "A review on device-free passive indoor positioning methods," *Int. J. Smart Home*, vol. 8, no. 1, pp. 71–94, 2014.

[26] Q. Wang and M. Zuniga, "Passive sensing and communication using visible light: Taxonomy, challenges and opportunities," 2017, *arXiv:1704.01331*. [Online]. Available: https://arxiv.org/abs/1704.01331

[27] Y. Yang, J. Hao, J. Luo, and S. J. Pan, "CeilingSee: Device-free occupancy inference through lighting infrastructure based LED sensing," in *Proc. IEEE Int. Conf. Pervasive Comput. Commun. (PerCom)*, Mar. 2017, pp. 247–256. doi: 10.1109/PERCOM.2017.7917871.

[28] M. Ibrahim, V. Nguyen, S. Rupavatharam, M. Jawahar, M. Gruteser, and R. Howard, "Visible light based activity sensing using ceiling photosensors," in *Proc. 3rd Workshop Visible Light Commun. Syst.*, Oct. 2016, pp. 43–48.

[29] E. D. Lascio, A. Varshney, T. Voigt, and C. Pérez-Penichet, "LocaLight: A battery-free passive localization system using visible light: Poster abstract," presented at the Proc. 15th Int. Conf. Inf. Process. Sensor Netw., Vienna, Austria, 2016.

[30] S. Zhang, K. Liu, Y. Ma, X. Huang, X. Gong, and Y. Zhang, "An accurate geometrical multi-target device-free localization method using light sensors," *IEEE Sensors J.*, vol. 18, no. 18, pp. 7619–7632, Sep. 2018.

[31] V. Nguyen, M. Ibrahim, S. Rupavatharam, M. Jawahar, M. Gruteser, and R. Howard, "Eyelight: Light-and-shadow-based occupancy estimation and room activity recognition," in *Proc. IEEE INFOCOM Conf. Comput. Commun.*, Apr. 2018, pp. 351–359. doi: 10.1109/INFOCOM.2018.8485867.

[32] T. Li, Q. Liu, and X. Zhou, "Practical human sensing in the light," presented at the Proc. 14th Annu. Int. Conf. Mobile Syst., Appl., Services, Singapore, Jun. 2016, pp. 71–84.

[33] T. Li, C. An, Z. Tian, A. T. Campbell, and X. Zhou, "Human sensing using visible light communication," in *Proc. 21st Annu. Int. Conf. Mobile Comput. Netw.*, Paris, France, Sep. 2015, pp. 331–344.

[34] S. Hu, Q. Gao, C. Gong, and Z. Xu, "Efficient visible light sensing in eigenspace," *IEEE Commun. Lett.*, vol. 22, no. 5, pp. 994–997, May 2018. doi: 10.1109/lcomm.2018.2808498.

[35] N. Faulkner, F. Alam, M. Legg, and S. Demidenko, "Smart wall: Passive visible light positioning with ambient light only," in *Proc. IEEE Int. Instrum. Meas. Technol. Conf. (I2MTC)*, Auckland, New Zealand, May 2019, pp. 1–6.

[36] Q. Zhang, C. H. Foh, B.-C. Seet, and A. C. M. Fong, "Location estimation in wireless sensor networks using spring-relaxation technique," *Sensors*, vol. 10, no. 5, pp. 5171–5192, 2010.

[37] W.-T. Yu, J.-W. Choi, Y. Kim, W.-H. Lee, and S.-C. Kim, "Self-organizing localization with adaptive weights for wireless sensor networks," *IEEE Sensors J.*, vol. 18, no. 20, pp. 8484–8492, Oct. 2018. doi: 10.1109/jsen.2018.2866053.

[38] F. Alam, N. Faulkner, M. Legg, and S. Demidenko, "Indoor visible light positioning using spring-relaxation technique in real-world setting," *IEEE Access*, vol. 7, pp. 91347–91359, 2019. doi: 10.1109/access.2019.2927922.

[39] D. Konings, B. Parr, F. Alam, and E. M.-K. Lai, "Falcon: Fused application of light based positioning coupled with onboard network localization," *IEEE Access*, vol. 6, pp. 36155–36167, 2018.

[40] J. Barraquand, B. Langlois, and J.-C. Latombe, "Numerical potential field techniques for robot path planning," *IEEE Trans. Syst., Man and*, vol. 22, no. 2, pp. 224–241, Mar. 1992.

[41] G. Li, Y. Tamura, A. Yamashita, and H. Asama, "Effective improved artificial potential field-based regression search method for autonomous mobile robot path planning," *Int. J. Mechatron. Autom.*, vol. 3, no. 3, pp. 141–170, 2013.

[42] H. Adeli, M. Tabrizi, A. Mazloomian, E. Hajipour, and M. Jahed, "Path planning for mobile robots using iterative artificial potential field method," *Int. J. Comput. Sci. Issues (IJCSI)*, vol. 8, no. 4, p. 28, Jul. 2011.

[43] A. Bhattacharyya, "On a measure of divergence between two statistical populations defined by their probability distributions," *Bull. Calcutta Math. Soc.*, vol. 35, no. 1, pp. 99–109, 1943.

[44] Y. Zhao, N. Patwari, J. M. Phillips, and S. Venkatasubramanian, "Radio tomographic imaging and tracking of stationary and moving people via kernel distance," in *Proc. 12th Int. Conf. Inf. Process. Sensor Netw.*, Philadelphia, PA, USA, Apr. 2013, pp. 229–240. doi: 10.1145/2461381.2461410.

[45] D. Konings, F. Alam, F. Noble, and E. M.-K. Lai, "Improved distance metrics for histogram-based device-free localization," *IEEE Sensors J.*, vol. 19, no. 19, pp. 8940–8950, Oct. 2019. doi: 10.1109/jsen.2019.2922772.

Daniel Konings (M'17) received the B.E. (Hons.) degree in computer systems and electronics engineering from Massey University, Auckland, New Zealand, in 2014, where he is currently pursuing the Ph.D. degree with the School of Food and Advanced Technology (SF&AT).

His research interests include indoor localization, digital signal processing, machine learning, IoT, and wireless sensor networks.

Nathaniel Faulkner received the B.E. (Hons.) degree in electronics and computer engineering from Massey University, Auckland, New Zealand, in 2016, where he is currently pursuing the Ph.D. degree.

His research interests include visible light positioning and the Internet of Things.

Fakhrul Alam (M'17–SM'19) received the B.Sc. (Hons.) degree in electrical and electronic engineering from BUET, Bangladesh, and the M.S. and Ph.D. degrees in electrical engineering from Virginia Tech, USA.

He is currently a Senior Lecturer with the School of Food and Advanced Technology (SF&AT), Massey University, New Zealand. His research interests include indoor localization, 5G and visible light communication, disaster management with 5G, IoT, and wireless sensor networks.

Dr. Alam is a member of the Institution of Engineering and Technology (IET).

Edmund M.-K. Lai (M'82–SM'95) received the B.E. (Hons.) and Ph.D. degrees in electrical engineering from The University of Western Australia in 1982 and 1991, respectively.

He has previously held faculty positions at universities in Australia, Hong Kong, and Singapore. He is currently a Professor of Information Engineering with the Auckland University of Technology, New Zealand. His research interests include digital signal processing, digital communications and networks, computational and swarm intelligence, and artificial neural networks.

Dr. Lai is a Fellow of the Institution of Engineering and Technology (IET).

Serge Demidenko (M'91–SM'94–F'04) graduated in computer engineering from the Belarusian State University of Informatics and Radio Electronics and the Ph.D. degree from the Institute of Engineering Cybernetics, Belarusian Academy of Sciences.

He is a Professor and the Dean of the School of Science and Technology, Sunway University, Malaysia. He is a Chartered Engineer in the U.K. He is also associated with the Department of Mechanical and Electrical Engineering, School of Food and Advanced Technology, Massey University, New Zealand. His research interests include electronic design and test, signal processing, instrumentation, and measurements.

Dr. Demidenko is also a Fellow of the IET.